# Effect of the entrance channel mass asymmetry on the limitation of light heavy-ion fusion cross sections

R. M. Anjos, V. Guimarães, N. Added, N. Carlin Filho,
M. M. Coimbra, L. Fante, Jr., M. C. S. Figueira, E. M. Szanto,
C. F. Tenreiro, and A. Szanto de Toledo
*Instituto de Física da Universidade de São Paulo, Departamento de Física Nuclear, Laboratório Pelletron, Caixa Postal 20516, 01498 São Paulo, São Paulo, Brazil*
(Received 26 June 1989; revised manuscript received 6 December 1989)

Evaporation residues resulting from the $^{11}B+^{27}Al$ and $^{19}F+^{19}F$ fusion reactions leading to the $^{38}Ar$ compound nucleus and from the $^{19}F+(^{12}C, ^{16}O, ^{27}Al, ^{40}Ca)$ reactions have been measured at incident energies 32 MeV $\leq E_L(^{19}F) \leq$ 72 MeV and 15 MeV $\leq E_L(^{11}B) \leq$ 50 MeV. The hindrance of the fusion cross sections, at energies above the interaction barrier, show a clear dependence on the entrance channel mass asymmetry. This dependence is discussed in terms of model predictions that treat explicitly the mass asymmetry degree of freedom.

## I. INTRODUCTION

The energy dependence of heavy-ion fusion reactions presents, for most of the systems experimentally investigated, an overall smooth behavior that permits the clear distinction of three energy regions, associated in the literature with different regimes.[1,2] Region I, identified at energies ranging from the interaction barrier height to two or three times its value is basically governed by the entrance channel potential barrier penetrability. In this case the relative motion can be treated classically by assuming phenomenological two-body forces (conservative as well as dissipative) that cause a trapping of the system in the attractive two-body effective potential, and is directly related to the entrance channel mass asymmetry. In the high-energy extreme, usually denominated region III, the fusion cross section is determined by the limited amount of angular momentum that the compound nucleus can assimilate. Rotating liquid drop model[3] (RLDM) calculations are successful in predicting the critical angular momentum characteristic of the fissioning compound nucleus. Recent refinements that allowed the incorporation of the effects of the finite range of the nuclear force and the diffuse nuclear surface have improved the predictions of the fission barriers.[4–6]

The intermediate region II, is somehow expected to reflect a smooth transition between the two adjacent regions, displaying an interplay between compound-nucleus[7] and entrance channel characteristics.[8] In order to isolate the chief limiting factor of the fusion cross section of light heavy-ion reactions, systematic studies have been performed. In the case of light compound nuclei, their small moment of inertia imposes an appreciable lower limit to the angular momentum necessary to absorb the available rotational energy by decreasing very rapidly the available high-spin states level density. Furthermore, for lighter systems, the weaker Coulomb repulsive interaction in the entrance channel makes its competition with the attractive nuclear potential less critical, although it is still sensitive to the entrance channel mass asymmetry. Within this scope it is reasonable to expect that compound-nucleus and entrance channel characteristics both influence the projectile-target amalgamation probability, and that the fusion cross section limitation results from the competition between fusion and other reaction processes. The entrance channel mass asymmetry dependence of some competing processes has been already clearly established. In the case of the emission of complex fragments, as well as the binary decay of highly excited composite systems this dependence has also been verified.[4,9,10] In a recent paper, Harmon *et al.*[11] showed that for the $^{40}Ca$ and $^{42}Ca$ and compound nuclei formed via different entrance channels, the extracted critical angular momentum at saturation ($l_c^{max}$) depends strongly on the entrance channel mass asymmetry indicating that at high energies, the largest angular momentum that the compound nucleus can sustain, before scission, is less when formed via a more asymmetric entrance channel. Furthermore, the strength of the incomplete fusion process, whose threshold is associated with the beginning of region II, has been shown to be strongly correlated with the entrance channel mass asymmetry.[12]

The amount of surface energy available in the system and the size of the neck that characterizes a dinuclear doorway configuration are related to the entrance channel mass asymmetry that also determines the relation between the composite system angular momentum and excitation energy. A quantitative study of the mass asymmetry dependence of the fusion cross section limitation is best accomplished by measuring the fusion cross section for several systems leading to the same compound nucleus, together with sets of measurements of systems in which one of the collision partners is maintained and the other is varied, covering a wide variety of systems. In the present work we investigated the $^{11}B+^{27}Al$ and $^{19}F+^{19}F$ fusion reactions leading to the $^{38}Ar$ compound nucleus and the $^{19}F+^{12}C$, $^{16}O$, $^{19}F$, $^{27}Al$, and $^{40}Ca$ reactions, thus allowing for an appreciable variation of the entrance channel mass asymmetry in the investigation of the influence of this specific degree of freedom in the fusion

 

cross section limitation.

A description of the experimental procedure and discussion are presented in Secs. II and III, respectively. Experimental results are compared with various models in Sec. IV and the conclusions are summarized in Sec. V.

## II. EXPERIMENTAL PROCEDURE

Beams of $^{11}B$ and $^{19}F$ ions were provided by the University of São Paulo Pelletron accelerator. The $^{11}B$ beam was accelerated over a laboratory energy range from 15 to 50 MeV, while the $^{19}F$ beam spanned an energy range from 32 to 72 MeV. Self-supporting $^{27}Al$ targets ($\approx 50$ $\mu g\,cm^{-2}$ thick) and $^{nat}Ca^{19}F_2$ (40 $\mu g\,cm^{-2}$ thick on $\sim 40$ $\mu g\,cm^{-2}$ aluminum backing) were used. A thin gold layer was deposited on the targets for normalization purposes. Carbon buildup during the exposures was minimized by surrounding the target with a liquid nitrogen cooled ring and using a cryogenic pumping system. However, unavoidable small $^{12}C$ and $^{16}O$ contaminations were monitored during the experiment. The evaporation residues were mass identified by measuring their time of flight along a 180 cm flight path, for the excitation function measurements, and along an $\sim 80$ cm flight path for the angular distribution measurements. A microchannel plate detector was used to detect the initial passage of the heavy residues that were then stopped in a 300 $mm^2$ silicon surface-barrier detector. The time resolution of 450 ps was sufficient to obtain unit mass resolution for all measured spectra, in the excitation functions. Evaporation residues from $^{19}F+^{40}Ca$ reaction were unresolved because of the energy resolution of the surface-barrier detector. The electronic thresholds did not impose any significant cutoff in the low bombarding energy spectra. Two-dimensional, time ($t$) versus energy ($E$), spectra were recorded on line simultaneously with $E$ and $t$ singles spectra for efficiency check purposes. Mass spectra, as shown in Fig. 1, were derived off line. Angular distributions were measured for the $^{11}B+^{27}Al$ systems from 5° to 40°in the laboratory at $E(^{11}B)=24$ MeV, 36 MeV, and 48 MeV and form 6° to 28° for the $^{19}F$ induced reactions at $E(^{19}F)=36$ MeV, 50 MeV, 64 MeV, and 72 MeV. Excitation functions were measured for all the systems in $\Delta E_{c.m.} \simeq 1.5$ MeV steps at a fixed angle $\theta_{lab}=7.5°$.

The evaluation of the fusion cross section was based on the analysis of the energy and velocity spectra of all residues masses individually in order to identify possible contributions attributed to quasielastic processes as well as from reactions with contaminants. Complete angular distributions, shown in Figs. 2(a) and (b), supplied, after angle integration, the total fusion cross section. At other energies, at which only the differential cross section $(d\sigma/d\Omega)_{\theta_M}$ at $\theta_M=7.5°$ has been measured, a smoothly interpolated relation

$$R=(d\sigma/d\Omega)_{\theta_M}/\int(d\sigma/d\theta)d\theta$$

has been used to deduce the total fusion cross section, fortified by the fact that this ratio $R$ varies slowly with bombarding energy. Absolute cross sections were determined by using the product of target thickness and detector solid angles derived from $\chi^2$ fits of the elastic scattering cross section to optical-model calculations. The uncertainty in the absolute total fusion cross section is estimated to vary from 10% to 15%. These values take into account counting statistics, extrapolation of the data to 0° and large angles, uncertainties in target thickness and detector solid angle and errors originated from the subtraction of the contaminant spectra.

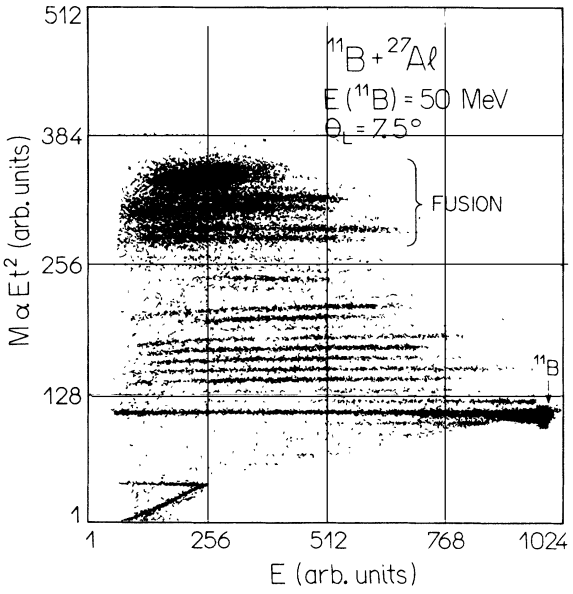


FIG. 1. Two-dimensional plot of the evaporation residues energy ($E$) vs the derived mass $M\alpha(Et^2)$, where $t$ represents the residue time of flight, for the $^{11}B+^{27}Al$ reaction at $E(^{11}B)=50$ MeV and $\theta_{lab}=7.5°$.

The subtraction of the contaminant contributions, when necessary, has been performed on the basis of individual mass spectra. In the case of the $^{11}B+^{27}Al$ reaction, the $^{16}O$ contamination gave no overlapping contribution with the evaporation residues of interest because of the large mass difference between target and contaminant. A more comfortable situation occurs with the low level of $^{12}C$ contamination. In the case of the $^{19}F+^{27}Al$ reaction, an analysis based on the characteristic mass distributions and sequential decay kinematics, allowed a clear identification of residues originating from the $^{19}F+^{27}Al$ and $^{19}F+^{16}O$ (contaminant) fusion reactions. In the case of $^{12}C$ contamination, the deconvolution of the very light evaporation residues spectra was further supported by a consistent analysis of velocity spectra and the results of the previously measured $^{19}F+^{12}C$ reaction reported in Ref. 13. In the case of the study of the $^{19}F+^{19}F$ reaction with $^{nat}CaF_2$ targets on $^{27}Al$ backing, the evaporation residues from the $^{19}F+Ca$ fusion reaction appeared isolated in the two-dimensional mass versus energy spectrum. Because of the fact that measurements on the $^{27}Al$ and $CaF_2$ targets were performed by alternating the targets, keeping all the other experimental conditions fixed, the spectra could be subtracted, in order to isolate the yield originating from the $^{19}F+^{27}Al$, $^{19}F+^{19}F$, $^{19}F+^{16}O$, and $^{19}F+^{12}C$ fusion reac-

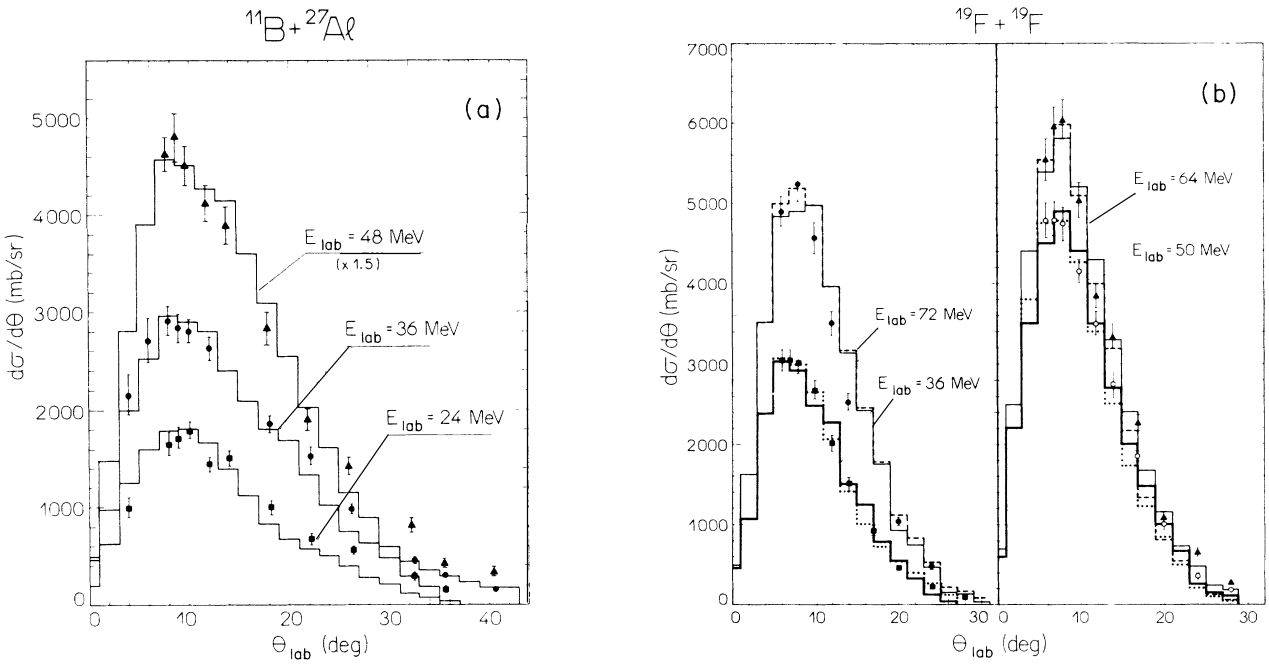


FIG. 2. Experimental angular distributions $(d\sigma/d\sigma) = 2\pi \sin\theta d\sigma/d\Omega$ of the evaporation residues for (a) the $^{11}B+^{27}Al$ reaction at $E(^{11}B)=24$ MeV, 36 MeV, and 48 MeV and (b) $^{19}F^{19}F$ reaction at $E(^{19}F)=36$ MeV, 50 MeV, 64 MeV, and 72 MeV. The histograms represent the prediction of Monte Carlo, Hauser-Feshbach calculations performed with the code PACE (Ref. 15) (solid lines) and LILITA (Ref. 16) (dashed and dotted lines).

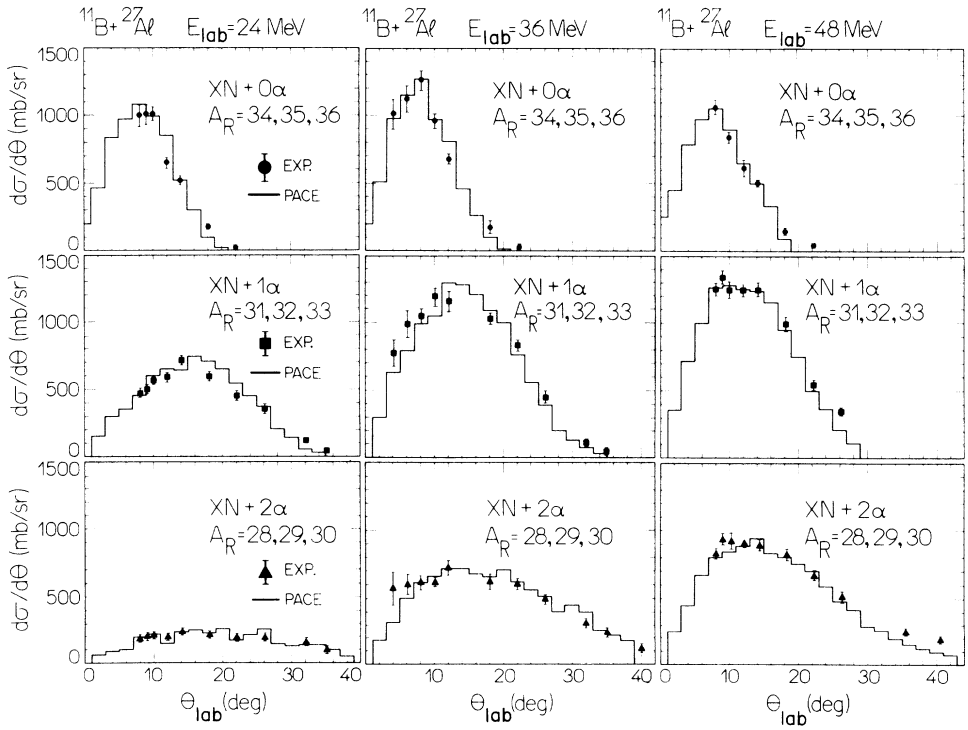


FIG. 3. Angular distributions for groups of three masses of the evaporation residues for the $^{11}B+^{17}Al$ reaction at 24 MeV, 36 MeV, and 48 MeV according to the number of alpha particles ($\alpha$) and nucleus ($N$) evaporated from the $^{38}Ar$ compound nucleus. The mass of the residues $A_R = 38-(XN+Y\alpha)$ are also indicted. The histogram represents the predictions of the code PACE for the indicated group of masses.

tions. At the energies used in the present work ($E/A \lesssim 4$ MeV/$\mu$), the velocity spectra of the evaporation residues appeared to be centered at the center-of-mass velocity, indicating that no significant contribution of incomplete fusion components is present. This finding is supported by the systematics for light systems, as a function of the entrance channel mass asymmetry established by Morgenstern *et al.*,[11] which predicts for the most asymmetric channel an incomplete fusion cross section estimated to be $\sigma_{ICF} \leq 0.03\sigma_{CF}$.

## III. EXPERIMENTAL RESULTS AND DISCUSSION

Angular distributions of the evaporation residues are shown in Fig. 3. The total fusion cross sections have been determined using the relation

$$\sigma_F(E) = \int_0^{\theta_{max}} 2\pi \sin\theta_L \left[ \frac{d\sigma}{d\Omega}(\theta_L, E) \right] d\theta_L \ . \quad (1)$$

To perform properly this integration the experimental angular distributions were extrapolated both to 0° and beyond the largest measured angle using a curve compatible with predictions based on statistical theory (see Fig. 2) for the considered angular interval, and reproduced by the empirical expression[14]

$$\frac{d\sigma}{d\theta} = a_1 \left[ \frac{\theta}{a_2} \right]^{a_3} \exp\left[ \frac{a_3}{a_4} \left[ 1 - \frac{\theta}{a_2} \right]^{a_4} \right] , \quad (2)$$

where the constants $a_i$ are determined by $\chi^2$ fits to the experimental angular distributions. This procedure decreases the systematic uncertainties.

Monte Carlo, Hauser-Feschbach calculations, which assumed neutron, proton, and alpha particle emission from the compound nucleus, were performed for both entrance channels with the computer codes PACE (Ref. 15) and LILITA (Ref. 16). A comparison of the experimental data with theoretical predictions is also shown in Figs. 2 and 3 and indicates good agreement as far as shape is concerned.

The kinematical broadening of the angular distribution increases with increasing total mass of evaporated particles revealing the increase of the resultant impulse that the residue suffers. This trend is perfectly reproduced by the theoretical calculations (see Fig. 3). The decay channels energetically available to the $^{38}$Ar compound-nucleus decay, indicated in Fig. 4, are correlated to the different energy thresholds for the opening of the possible exit channels associated with the emission of a particular number of light particles (only $n$, $p$, and $\alpha$ particles are considered because of the low cross section expected for the emission of $d$, $t$, $^3$He particles and heavier clusters).

Figure 5 shows the experimental excitation functions for the evaporation residues, whose main trends can be understood in term of the competition between the energetically allowed decay channels as indicated in Fig. 4. The difference in mas asymmetry of the $^{11}$B+$^{27}$Al and $^{19}$F+$^{19}$F entrance channels and in their $Q$ values for the $^{38}$Ar compound-nucleus formation determines that, at the same center-of-mass energy, the $^{38}$Ar compound-nucleus angular momentum distribution and excitation energy will be different for both entrance channels, leading to different probabilities in the population of a given decay channel. This fact, taken into account properly in the calculated total cross sections and mass distributions, justifies the good agreement between experimental and theoretical excitation functions (see Fig. 5).

The energy dependence of the total fusion cross section, for all the reactions investigated in the present work are presented in Fig. 6. $\chi^2$ fits to the Glas and Mosel model[8,17] allow the extraction of the fusion barrier parameters $V_B$ (barrier height) and $R_B$ (barrier radius) listed in Table I. These values agree satisfactorily with systematics proposed by Kovar *et al.*[21] Fits to the predictions of semiclassical calculations of barrier penetration described by the proximity potential[22] are also presented in Fig. 6. In this case only the radii of the interacting nuclei ($R = R_0 + \Delta R$) were varied resulting in a less satisfactory overall agreement.

Plots of the compound-nucleus excitation energy ($E^*_{c.m.}$) vs the critical angular momentum squared [$l_c(l_c+1)$], presented in Fig. 7, show different trajectories for the two systems indicating that at the highest energies measured, in spite of the fact that the compound nucleus is populated for the different channels at comparable tem-

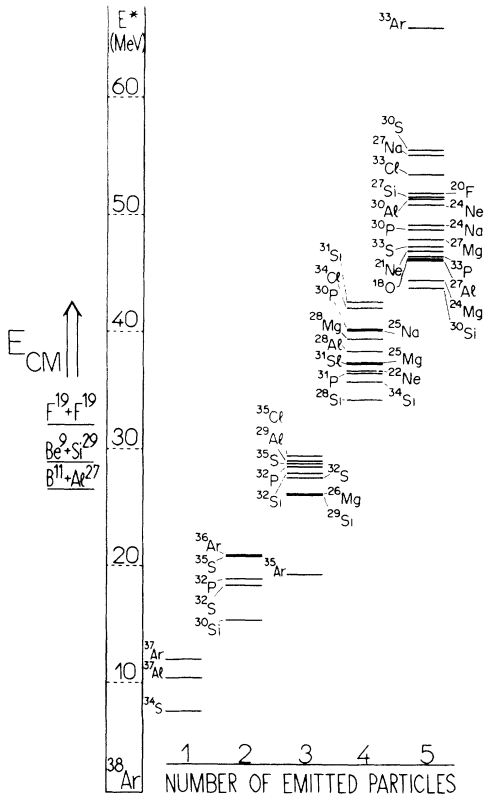


FIG. 4. Decay channels energetically available for the $^{38}$Ar compound nucleus. The different evaporation residue groups are formed in terms of number of particles emitted (i.e., $n$, $p$, or $d$).

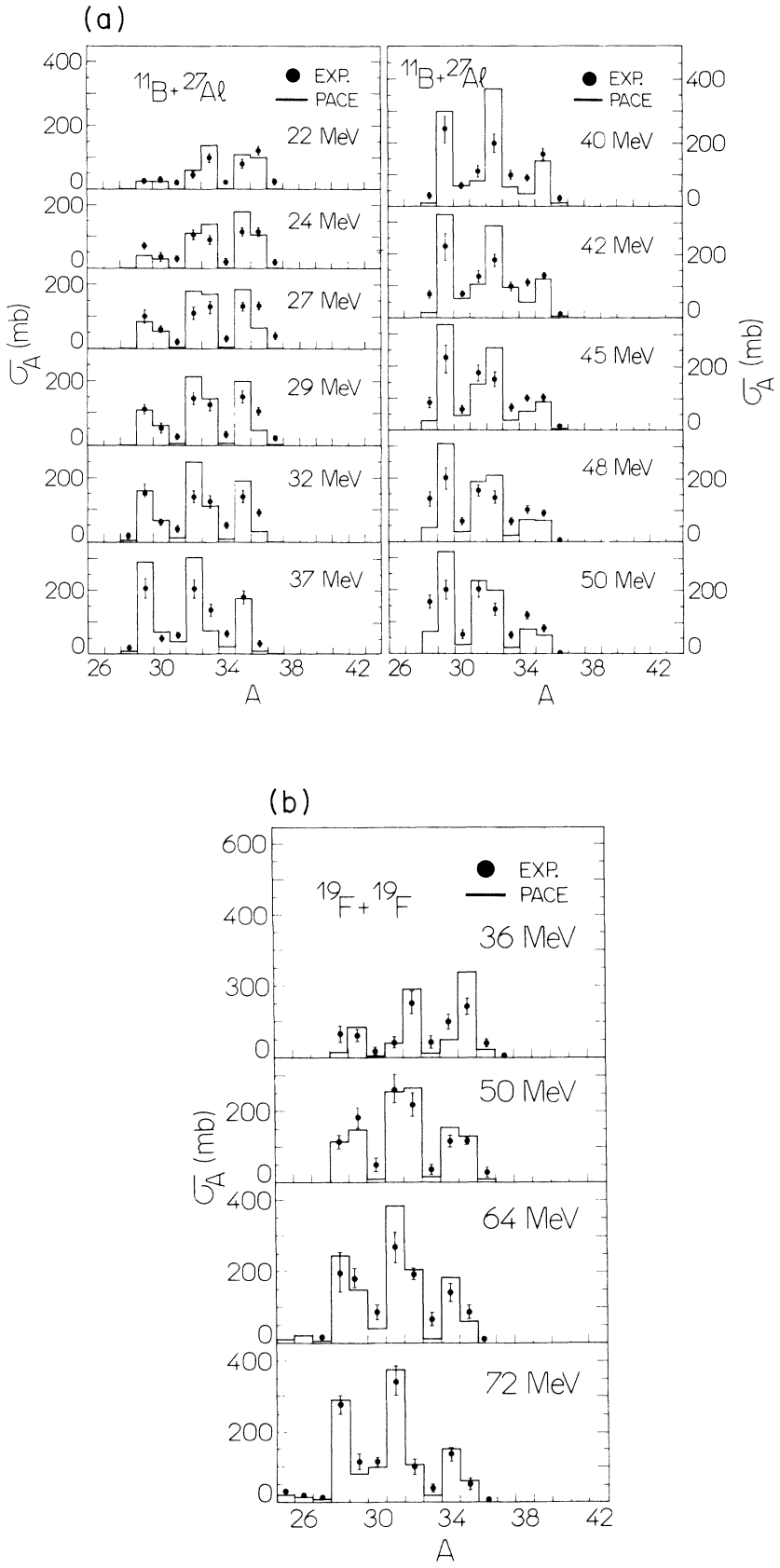


FIG. 5. Energy dependence of the evaporation residues cross sections for the $^{11}B+^{27}Al$ reaction (upper) and $^{19}F+^{19}F$ reaction (lower). The theoretical predictions are represented by the histograms.

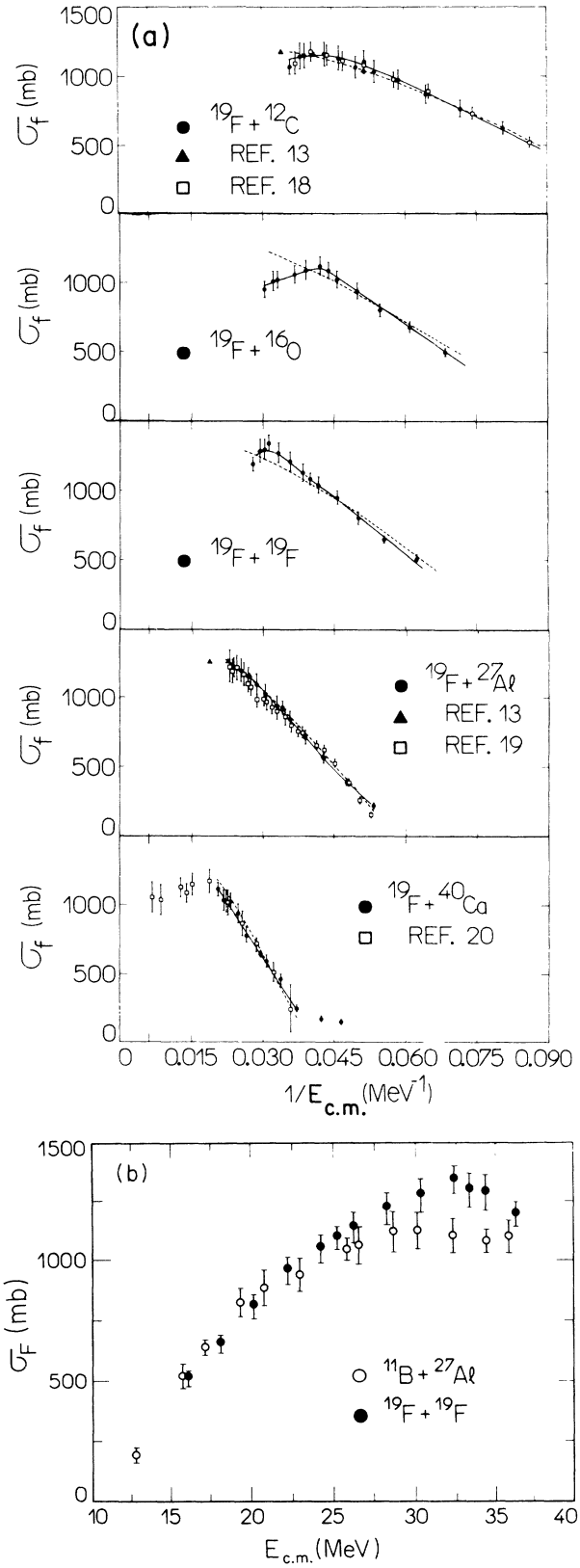


FIG. 6. (a) Total fusion cross sections ($\sigma_f$) for the ($^{19}F+^{12}C$), ($^{19}F+^{16}O$), ($^{19}F+^{19}F$), ($^{19}F+^{27}Al$), and ($^{19}F+^{40}Ca$) systems as a function of the inverse of the energy ($E_{c.m.}$). Solid lines represent fits to the Glas and Mosel model (Ref. 8) and the dashed lines represent predictions based on the barrier penetrability of a proximity potential (Ref. 22). Data found in the literature, for these systems are also presented, i.e., Pulhofer *et al.* (Ref. 13), Sperr *et al.* (Ref. 18), Chiou *et al.* (Ref. 19), and Rosner *et al.* (Ref. 20). (b) Comparison of the excitation functions for the two reactions leading to the $^{38}Ar$ compound nucleus showing the different behaviors at higher bombarding energies.

TABLE I. Fusion barrier parameters obtained in the present work.

| System | $R_B$ (fm) | $V_B$ (MeV) |
|---|---|---|
| $^{19}F+^{12}C$ | 7.89 | 8.51 |
| $^{19}F+^{16}O$ | 8.23 | 11.21 |
| $^{19}F+^{19}F$ | 8.30 | 12.44 |
| $^{19}F+^{27}Al$ | 8.40 | 17.54 |
| $^{19}F+^{40}Ca$ | 8.41 | 24.09 |
| $^{11}B+^{27}Al$ | 7.84 | 11.44 |

peratures, the critical angular momentum deviates continuously from the grazing angular momentum in the $^{11}B+^{27}Al$ case but shows an abrupt increase in the higher energies for the symmetrical $^{19}F+^{19}F$ case.

## IV. THE MASS ASYMMETRY DEGREE OF FREEDOM

Models based on one-dimensional barrier penetrability are able to predict fusion cross sections which, in region I, are determined basically by the barrier height ($V_B$) and radius ($R_B$) and represented by the relation

$$\sigma_F(E_{c.m.})=\pi R_B^2\left[\frac{E_{c.m.}-V_B}{E_{c.m.}}\right] . \tag{3}$$

A reduced fusion cross section $\sigma_F^{red}$ can be determined and associated with the available energy above the barrier

$$\sigma_F^{red}=\frac{\sigma_F\cdot E_{c.m.}}{\pi R_B^2}=(E_{c.m.}-V_B) . \tag{4}$$

With such a renormalization, the fusion cross section for all the systems coincide in region I, after removing the main dependence on the geometrical constraints, and thus allowing the enhancement of particular dynamical effects of the collision. As seen in Fig. 8, the reduced cross section varies linearly as a function of the energy above the barrier ($E_{c.m.}-V_B$) with a slope of 45°. With increasing bombarding energies, when larger values of the orbital angular momentum ($l\hbar$) are involved, faster and more peripheral reaction channels are opened, thus leading to an inhibition of the fusion cross section with respect to barrier penetrability cross section as a result of the competition between the several opened channels. In Fig. 9, this effect is represented by a new line, deviating from the former one by an angle $\alpha$. A fusion inhibition factor (FIF=tan$\alpha$) is defined and determined for the systems investigated in this work. A correlation between the fusion inhibition factor and mass asymmetry

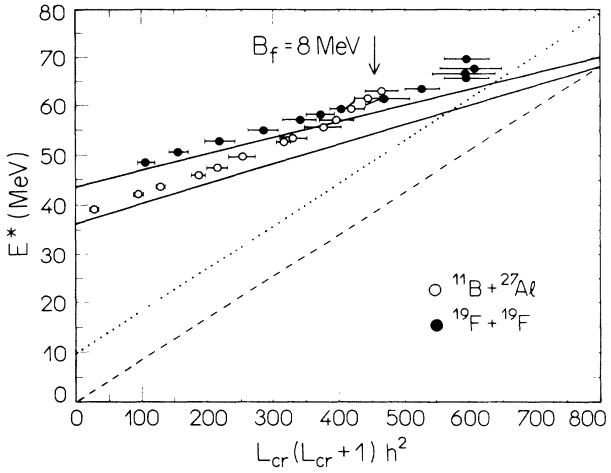


FIG. 7. Excitation energy of the $^{38}Ar$ compound nucleus versus the critical angular momentum squared for fusion, determined in the ($^{11}B+^{27}Al$) and ($^{19}F+^{19}F$) reactions. The yrast line (dashed line), trajectory of the grazing angular momentum squared $[l_g(l_g+1)]$ (solid lines) and the statistical yrast line (Ref. 7) are also indicated. The critical angular momentum for which the fission barrier $B_f$ is reduced to 8 MeV is indicated by the arrow.

$$\eta=(A_H-A_L)/A_H+A_L$$

[where $A_H(A_L)$ represent the mass of the heavy (light) partner of the entrance channel] appears clearly in Fig. 10 indicating that asymmetrical entrance channel clearly favors fusion. It should be noted that the values for FIF, extracted from our data, even at the highest energies, reflect the trend of the inclusive fusion cross section, which includes complete and incomplete fusion processes without distinction. However, as mentioned earlier, the influence of the incomplete fusion components in our data is negligible. Very similar correlations to the one shown in Fig. 10 can be found for the data available in the literature.[24,26] In these cases, most of the fusion cross section values are found in the inclusive form because in very few cases has the contribution of incomplete fusion processes been identified and subtracted. In region I, a similar feature can be observed for the absolute cross section as a result of the balance between the repulsive Coulomb force and the attractive nuclear force, which may be described by a proximity potential. Figure 11 shows the dependence of the effective fusion barrier $V_B$, predicted by a proximity potential,[22] with the entrance channel mass asymmetry parameter $\eta$. The fusion of systems with large mass asymmetry allow the formation of compound nuclei with lower excitation energy because of the smaller Coulomb contribution to the fusion barrier. Recently Carjan *et al.*[23] calculated fusion barriers for a heavier compound system and his results when compared to empirical systematics indicated a correlation with $\eta$ similar to the one observed in Fig. 11.

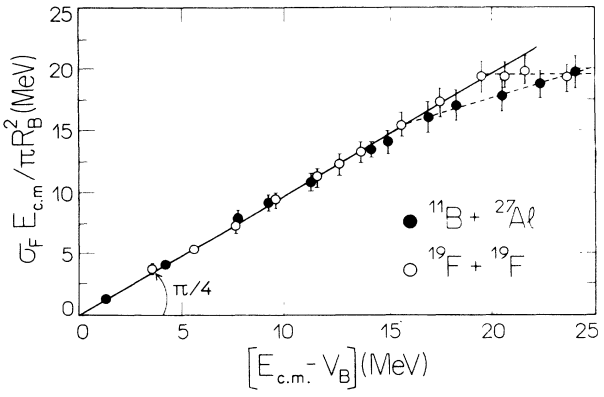


FIG. 8. Reduced fusion cross sections [see expression (4)] of the ($^{11}B+^{27}Al$) and ($^{19}F+^{19}F$) systems. The dashed lines represent linear fits to the high-energy data.

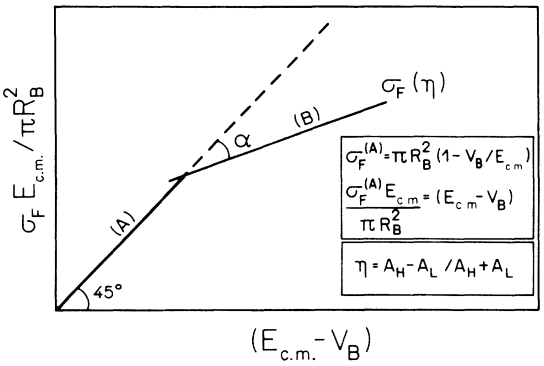


FIG. 9. Schematic description of the reduced fusion excitation function indicating the deviation from the behavior determined, in region ($A$), by the penetrability of the entrance channel barrier. Region ($B$) is represented by a new line which deviates by an angle $\alpha$ from the former trajectory.

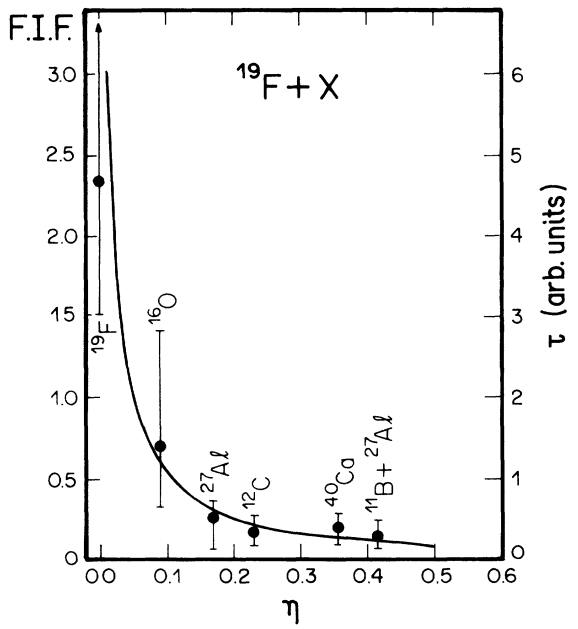


FIG. 10. Fusion inhibition factor (FIF) obtained for the systems investigated in the present work, as a function of the entrance channel mass asymmetry $\eta$. The solid line dependence of the configuration life time ($\tau$), described in the text and predicted by the liquid drop model, as a function of the mass asymmetry.

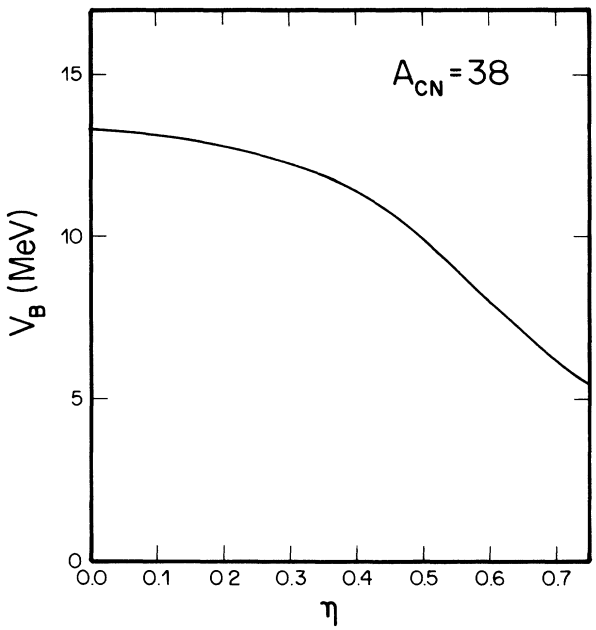


FIG. 11. Fusion barrier height $V_B$, predicted by a proximity potential for the $^{38}$Ar compound-nucleus formation as a function of the entrance channel mass asymmetry. In these calculations, the atomic number ($Z$) of the colliding elements was supposed to be half of their atomic mass ($A$).

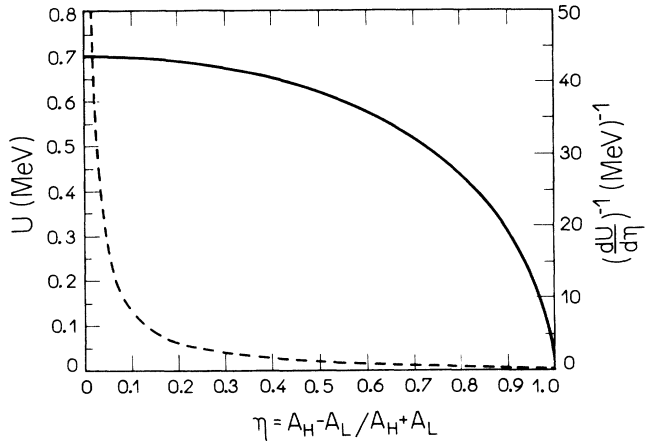


FIG. 12. Calculated values for the "driving potential" $U$ as a function of the mass asymmetry of the initial system, for an $A=38$, $Z=18$ compound nucleus (solid line). The dashed line represents the value of $(dU/d\eta)^{-1}$ associated to "configuration life time" $\tau$.

It should be mentioned that the study performed by Harmon *et al.*[11] indicates that the saturation of the critical angular momentum for the production of evaporation residues, in the case of the $^{40}$Ca and $^{42}$Ca compound nuclei, occurs at lower $l$ values when the entrance channel mass asymmetry is higher. This study corresponds to one of the few fusion excitation functions found in the literature where the incomplete fusion cross section has been systematically subtracted and consequently cannot be compared with the other systems on the same grounds. The FIF factors extracted from this work are the ones with the largest discrepancy within our systematics. However, if the inclusive fusion excitation functions are reconstructed, the results tend to fit into the systematics of Fig. 10. On the other hand, a very similar study for the systems $^{16}$O+$^{40}$Ca and $^{28}$Si+$^{28}$Si leading to the compound nucleus $^{56}$Ni presented by Hinnefeld *et al.*[24] allow the extraction of fusion inhibition factors which fit perfectly in our systematics.

From the liquid drop model, the ground-state energy of the target, projectile and compound nucleus may be calculated as well as the energy released for formation of the compound nucleus. This energy is referred as a "driving potential" ($U$) and is calculated as a function of the mass asymmetry of the initial system. The dependence of $U(A_1, A_2)$ with $\eta$ is shown in Fig. 12 for a system ($A_1+A_2=38$), ($Z_1+Z_2=18$). Starting from any initial configuration $\eta_0$ the system will be driven towards decreasing values of $U$. The derivative $\partial U/\partial\eta$ can be associated with a "restoring force" driving the system to a final configuration. The inverse function $\tau=(\partial U/\partial\eta)^{-1}$ can therefore be related to an average "configuration life time."

The larger the value of $\tau$, the longer the system will remain in this configuration, thus, increasing the relative probability of decay into a similar symmetric exit channel with consequent removal of flux from the complete fusion channel. Figure 10 shows that FIF and $\tau$ have very similar behavior with respect to $\eta$. This feature is observed when a given compound nucleus is populated via several entrance channels varying the mass asymmetry (in our case $A_{CN}=38$), or when one colliding partner is maintained fixed and the other is varied (i.e., $^{19}$F+$X$). This behavior indicates that the entrance channel mass asymmetry degree of freedom is relevant in the determination of the fusion cross section limitation at energies above the interaction barrier, even in the case of lighter systems for which the liquid drop model predictions may carry large uncertainties.[25]

## V. SUMMARY

The dependence of the properties of nuclei during fission, fusion, and other processes on the mass asymmetry is of great importance. The understanding of the correlation between this degree of freedom and the collision dynamics may enable one to characterize or distinguish several reaction mechanisms as, for example, in the case of the asymmetric binary decay of a composite system following the equilibrated compound-nucleus formation or a fast fission process.

We have investigated the effect of the entrance channel mass asymmetry on the limitation of light heavy-ion fusion cross section. Evaporation residues from the ($^{19}$F+$^{19}$F) and ($^{11}$B+$^{27}$Al) reactions were detected as well as from the ($^{19}$F+$^{12}$C, $^{16}$O, $^{27}$Al, and $^{40}$Ca) systems. A clear dependence of the fusion inhibition factor (FIF) on the mass asymmetry parameter $\eta$ has been established.

Calculations based on proximity potentials and on the

liquid drop model were used to establish a dependence of the fusion barrier and "driving potential" to asymmetry configurations, with the entrance channel mass asymmetry suggesting that an increase of the FIF should be expected with increasing symmetry in the entrance channel.

## ACKNOWLEDGMENTS

This work was supported in part by Fundação de Amparo à Pesquisa do Estado de São Paulo (FAPESP) and by Conselho Nacional de Desenvolvimento Científico e Tecnológico.

[1]J. R. Birkelund and J. R. Huizenga, Annu. Rev. Nucl. Sci. **33**, 265 (1983), and references therein.

[2]U. Mosel, in *Heavy Ion Collisions,* edited by R. Bock (North-Holland, Amsterdam, 1980), Vol. 2, p. 275.

[3]S. Cohen, F. Plasil, and W. J. Swiatecki, Ann. Phys. (N.Y.) **82**, 557 (1974).

[4]A. J. Sierk, Phys. Rev. Lett. **55**, 582 (1985); Phys. Rev. C **33**, 2039 (1986).

[5]M. G. Mustafa, P. A. Baisden, and H. Chandra, Phys. Rev. C **25**, 2524 (1982).

[6]K. Grotowski, R. Planeta, M. Blann, and T. Komoto, Phys. Rev. C **39**, 1320 (1989), and references therein.

[7]O. Civitarese, B. V. Carlson, M. S. Hussein, and A. Szanto de Toledo, Phys. Lett. **125B**, 22 (1983).

[8]D. Glas and V. Mosel, Nucl. Phys. **A237**, 429 (1975).

[9]W. V. Schröder and J. R. Huizenga, Annu. Rev. Nucl. Sci. **27**, 465 (1977).

[10]M. A. McMahan, L. G. Moretto, M. L. Padgett, G. J. Wozniak, L. G. Sobotka, and M. G. Mustafa, Phys. Rev. Lett. **54**, 1995 (1985).

[11]B. A. Harmon, D. Shapira, P. H. Stelson, B. L. Burks, K. A. Erb, B. Shivakumar, K. Teh, and S. T. Thornton, Phys. Rev. C **38**, 572 (1988); B. A. Harmon, S. T. Thornton, D. Shapira, J. Gomes del Campo, and M. Beckerman, *ibid.* **34**, 552 (1986).

[12]H. Morgenstern, W. Bohne, W. Galster, K. Grabisch, and A. Kyanowski, Phys. Rev. Lett. **52**, 1104 (1984).

[13]F. Puhlhofer, Nucl. Phys. **A280**, 267 (1977).

[14]R. Liguori Neto, private communication.

[15]A. Gavron, Phys. Rev. C **21**, 230 (1980).

[16]J. Gomez del Campo, R. G. Stokstad, J. A. Biggerstaff, R. A. Dayras, A. H. Snell, and P. H. Stelson, Phys. Rev. C **19**, 2170 (1979).

[17]C. Y. Wong, Phys. Rev. Lett. **31**, 766 (1973).

[18]P. Sperr, T. H. Braid, Y. Eisen, D. G. Kovar, F. W. Prosser, Jr., J. P. Schiffer, S. L. Tabor, and S. Vidgor, Phys. Rev. Lett. **37**, 321 (1976).

[19]M. S. Chiou, M. W. Wu, N. Easwar, and J. V. Maher, Phys. Rev. C **24**, 447 (1983).

[20]G. Rosner, J. Pochodzalla, B. Heck, G. H. Lawatsch, A. Miczaika, H. J. Rabe, R. Butsch, and B. Sedelmeyer, Phys. Lett. **150B**, 87 (1985).

[21]D. G. Kovar, D. F. Geesaman, T. H. Braid, Y. Eisen, W. Henning, T. R. Ophel, M. Paul, K. E. Rehm, S. J. Sanders, P. Sperr, J. P. Schiffer, S. L. Labor, S. Vidgor, and B. Zeidman, Phys. Rev. C **20**, 1305 (1979).

[22]J. Blocki, J. Randrup, W. J. Swiatecki, and C. F. Tisang, Ann. Phys. (N.Y.) **105**, 427 (1977).

[23]N. Carjan and J. M. Alexander, Phys. Rev. C **38**, 1692 (1988).

[24]J. D. Hinnefeld, J. J. Kolata, D. J. Henderson, R. V. F. Janssens, D. G. Kovar, K. T. Lesko, G. Rosener, F. W. Prosser, and S. V. Reinert, in Proceedings of the Symposium on *Many Facets of Heavy-Ion Fusion Reactions,* Argonne National Laboratory, 1986, edited by W. Henning, D. Kovar, S. Landowne, and S. Pieper (unpublished), p. 525.

[25]J. Blocki, K. Grotowski, R. Plancta, and W. J. Swiatecki, Nucl. Phys. **A445**, 367 (1985).

[26]K. Blatt, in Proceedings of the Symposium on *Many Facets of Heavy-Ion Fusion Reactions,* Argonne National Laboratory, 1986, edited by W. Henning, D. Kovar, S. Landowne, and S. Pieper (unpublished), p. 433, and references therein.